LBNL-55103
May 2004

Longitudinal Single-Bunch Instabilities in the NLC Main Damping Rings*

M. Venturini
Lawrence Berkeley National Laboratory,
Berkeley, CA, 94720.

Abstract

Because of tight requirements on beam quality longitudinal single-bunch instabilities are a serious concern for the damping rings of the next generation of linear colliders. Unlike multi-bunch instabilities they cannot be damped using feedback systems and need to be avoided altogether. We present an analysis of these instabilities for the current (Feb. 03) NLC main damping ring design, with attention paid to coherent synchrotron radiation and vacuum chamber effects, with the latter including the main components (RF cavities, BPM's, and resistive wall). The study is carried out by solving the Vlasov-Fokker-Planck equation for the longitudinal motion numerically. Comparison is made, whenever possible, with linear theory. We find that collective effects are dominated by coherent synchrotron radiation and estimate the instability threshold to be safely above 6 times the design current.

*Work supported by Department of Energy contract DE-AC03-76SF00098.

1 Introduction

The NLC main damping rings (MDR) lattice was redesigned last year to increase the momentum compaction [1, 2]. This was in response to estimates of collective effects that had placed the threshold for instability close to the working point: a larger momentum compaction eases the collective forces as it lengthens the bunches (therefore diluting the charge density) and boosts Landau damping.

Coherent synchrotron radiation effects (CSR), in particular, were found to be the most offensive. These had not been considered in the last reported survey of collective limitations, the 1996 NLC "Zeroth Order Design" Report (ZDR) [3]. Indeed, while awareness that CSR could cause instability is relatively old, only recently has appreciation of its dynamical effects started to emerge – mostly as a result of the experience with designing bunch compressors and, more recently, measurements of CSR bursts in light sources.

Our goal here is to update the study of single-bunch longitudinal collective instabilities reported in [3] to account for CSR and the subsequent changes in the MDR lattice. A recent assessment of CSR, including effects from both the bending magnets and wiggler insertions, was reported in [4] but there the analysis focused mostly on the pre-February 2003 MDR lattice with smaller momentum compaction. In this Report we update and complement [4], by making reference to the latest MDR design and using a model of shielded impedance for the CSR effects in the dipoles (whereas a free-space impedance model is used in [4]). Moreover, we supplement the analytical study of linear stability with time-domain numerical solutions of the Vlasov-Fokker-Planck equation for the longitudinal motion and fully account for radiation damping and beam bunching.

We also analyze the collective effects rising from the vacuum chamber, with attention paid to resistive wall, RF cavities and beam position monitors (BPM), *i.e.* the sources of impedance already considered in the stability analysis reported in [3]. The overall effect of other components (*e.g.* slots, masks, injection and extraction kickers, etc.) is believed to be relatively less important and will be included at a later time.

The vacuum chamber effects are modelled by wake functions computed numerically using 3D em codes. The specific wakes used for the present study differ from those originally used for the ZDR study as they reflect a later modification in the pipe radius from $b = 1.25$ cm to 1.6 cm. Although at present the value for the prevalent (70%) vacuum chamber radius is expected to be yet larger ($b = 2$ cm) we deemed appropriate at this stage to use the latest available determination for wakes although carried out at the smaller ($b = 1.6$ cm) radius. Bunch stability analysis of the vacuum chamber wakes was also conducted by solving the VFP equation numerically.

The content of the paper is as follows. In the next section we remind the reader of the basic equations for the longitudinal motion and report the dispersion relation for coasting beams which is often used for a first assessment of linear stability. In Section 3 we review models for radiation impedances for both dipoles and wigglers and use them to study instability. In Section 4 we study the effect of the main vacuum chamber components. Finally, in the Appendix we apply our methods to study the effects of the vacuum chamber components in the old 1996 MDR lattice design to make contact with the analysis reported in [3], which

was carried out using with different tools.

MKS units are used throughout if not otherwise stated.

2 Equations of Motion and Notation

We describe the longitudinal motion using the pair of coordinates z, the position with respect to the synchronous particle, and $\Delta E/E_0 = (E - E_0)/E_0$ the relative energy deviation from the design value. We define the slippage factor as $\eta = \alpha - 1/\gamma_0^2$, so that η is positive above transition for a standard lattice design. Let T_0 be the revolution time for an on-energy particle, C the ring circumference and β_0 the relativistic factor ($c\beta_0 = C/T_0$). The equations for the longitudinal motion read

$$\frac{dz}{dt} = -\frac{c\eta}{\beta_0}\frac{\Delta E}{E_0}, \tag{1}$$

$$\frac{d}{dt}\left(\frac{\Delta E}{E_0}\right) = -\frac{eV(z)}{T_0 E_0}, \tag{2}$$

where $V(z) = V_{\rm rf}(z) + V_c(z)$ is the voltage difference experienced by a particle through one machine revolution. The term

$$V_{\rm rf}(z) = -z\frac{h_n}{R_{\rm av}}\hat{V}\cos\phi_s, \tag{3}$$

valid for small z, represents the voltage kick contributed by passage through the RF cavity (or cavities) where $\hat{V}$ is the peak RF-voltage, ϕ_s the synchronous phase, $h_n = \omega_{\rm rf}/\omega_0$ the harmonic number, and $R_{\rm av}$ the ring average radius. For small currents only $V_{\rm rf}$ contributes to the voltage. By combining (1) and (2), $\ddot{z} = -\omega_s^2 z$, and from (3) the resulting expression for the synchrotron oscillation frequency is $\omega_s^2 = \omega_0^2(eh_n\hat{V}|\eta\sin\phi_s|/2\pi E_0\beta_0^2)$, where $\omega_0 = 2\pi/T_0$ is the revolution frequency. For stability it is understood that $\eta\sin\phi_s > 0$. From now on we assume, as is the case for the MDR, to be above transition, $\eta > 0$.

In addition to $V_{\rm rf}$ a particle can experience a beam induced voltage V_c resulting from the interaction with the other particles in the bunch. The interaction can occur directly through radiation or Coulomb forces, or can be mediated through the surrounding machine environment (wake fields). Either way, V_c can be described in terms of a "wake potential" function $W(z - z')$

$$V_c(z) = -eN\int W(z - z')\rho(z')dz', \tag{4}$$

where N is the number of particles per bunch and $\rho(z)$ the longitudinal density with normalization $\int \rho(z)dz = 1$. Specifically, $W(z - z')/C$ has the meaning of longitudinal electric field per unit charge (averaged along the ring circumference C) at point z due to a unit charge located at point z', *i.e.* $W(z - z')$ has dimensions of voltage over charge; in this paper we set the sign of $W(z - z')$ by the convention that a positive value corresponds to energy gain

Table 1: Relevant Parameters for the MDR Current (Feb. 2003) Design.

Description	Notation	Value
Energy	E_0	1.98 GeV
Rigidity	$Brho$	6.604 Tm
Ring circumference	C	300 m
Average ring radius	$R_{\rm av}$	47.75 m
Revolution frequency	$\omega_0/2\pi$	1 MHz
Pipe radius (except wiggler sections)	b_a	2 cm
Pipe radius in wiggler sections	b_w	0.8 cm
Conductivity of pipe (Al)	σ	$3.5 \times 10^7\ \Omega^{-1}\mathrm{m}^{-1}$
Radius of curvature in dipoles (CSR calc.)	R_d	10 m
Chamber height (CSR calc.)	h	4 cm
Momentum compaction	α	1.388×10^{-3}
Synchrotron frequency	$\omega_s/2\pi$	11.8 KHz
Synchrotron tune	ν_s	0.0118
Natural bunch length	σ_{z0}	5.5 mm
Natural rms relative energy spread	$\sigma_{\delta 0}$	0.975×10^{-3}
Longitudinal damping time	τ_d	2.18 ms
Harmonic number	h_n	714
RF voltage	$\hat{V}_{rf}$	2.0 MV
RF frequency	$\omega_{\rm rf}/2\pi$	714 MHz
Number of cavities		4
No. of BPM's (tentative)		146
Wiggler period	λ_w	0.27 m
Wiggler wave number	k_w	23.2711 m^{-1}
Wiggler peak field	B_{w0}	2.1 T
Wiggler parameter	K	53
Wiggler fundamental wave number	k_0	$4.98 \times 10^5\ \mathrm{m}^{-1}$
Total length of wiggler insertions	L_w	62 m
Radius of orbit in wigglers at $B = B_{w0}$	R_w	3.3 m
Bunch population	N	0.75×10^{10}

(this is opposite of the definition by Chao [5], where a positive sign corresponds to energy loss). To avoid possible confusion one should be alerted that in Refs.[4, 6, 7], $W(z-z')$ is used to denote a wake potential *density* and has dimension of electric field per unit charge.

The frequency domain companion of the wake potential is the impedance defined as[†]

$$Z(k) = -\frac{1}{c\beta_0}\int_{-\infty}^{\infty} dz W(z) e^{-ikz}. \tag{5}$$

The limits of integrations can be safely pushed to $\pm\infty$ as for the wakes of interest for single-bunch instabilities $W(z)$ becomes negligible for $|z| > z_c$, where z_c is a small fraction of the ring circumference.

Conversely

$$W(z) = -\frac{c\beta_0}{2\pi}\int_{-\infty}^{\infty} dk e^{ikz} Z(k). \tag{6}$$

In terms of impedance the collective contribution V_c to the voltage reads

$$V_c(z) = eNc\beta_0 \int dk e^{ikz} Z(k)\hat{\rho}(k), \tag{7}$$

with the Fourier transform of the charge density defined as $\hat{\rho}(k) = \int dz e^{-ikz}\rho(z)/2\pi$.

It is often convenient to express (6) and (7) in terms of Fourier series rather than Fourier integrals. In some way this is a more physically appropriate description because of the natural periodicity represented by the ring circumference. However, because the latter is so much larger than the bunch length the two descriptions are, in practice, equivalent.

We discretize the wave number k by setting $k = n/R$. A natural choice for R is the ring average radius $R = R_{\rm av} = C/(2\pi)$, but any choice for R is legitimate as long as R is much larger than the bunch length. In the following we will exploit this freedom. Having defined $\rho_n = \hat{\rho}(k = n/R)$ and $\tilde{Z}(n) = Z(k = n/R)$ the beam-induced potential difference can be written as

$$V_c(z) = eN\hat{\omega}_0 \sum_{n=-\infty}^{\infty} e^{inz/R}\tilde{Z}(n)\rho_n, \tag{8}$$

where we have introduced $\hat{\omega}_0 = c\beta_0/R$. Notice that in general $\hat{\omega}_0 \neq \omega_0$ unless $R = R_{\rm av}$.

To make contact with the notation in [6] we re-write the equations by rescaling the dynamical variables. Having introduced the natural relative energy spread $\sigma_{\delta 0} = \langle(\Delta E)^2\rangle^{1/2}/E_0$ (the rms spread of a bunch at equilibrium in the low-current limit) we write the relative energy deviation in units of $\sigma_{\delta 0}$, $\tilde{p} = (\Delta E/E_0)/\sigma_{\delta 0}$. By choosing the arc-length position of the bunch along the ring $s = c\beta_0 t$ as the independent variable we obtain for the equations of motion:

$$\frac{dz}{ds} = -\frac{\eta\sigma_{\delta 0}}{\beta_0^2}\tilde{p}, \tag{9}$$

$$\frac{d\tilde{p}}{ds} = -\frac{e}{CE_0\sigma_{\delta 0}}\left[V_{\rm rf}(z) + V_c(z)\right]. \tag{10}$$

[†]The minus sign is introduced so that the resulting impedance agrees with standard usage [5].

As an alternate way to write the equations we scale z with respect with σ_{z0}, the rms bunch length in the low-current limit, *i.e.* $q = z/\sigma_{z0}$. In the low current limit a bunch of electrons in a high energy storage ring reaches an equilibrium in the form of a gaussian distribution and the quantities $\sigma_{\delta 0}$ and σ_{z0} are related by $\nu_s \beta_0 (\sigma_{z0}/R_{\rm av}) = |\eta| \sigma_{\delta 0}$ where $\nu_s = \omega_s/\omega_0$ is the synchrotron tune. Keeping in mind this relationship, by using the scaled time $\tau = \omega_s t$ as the independent variable, and defining $p = -\Delta E/E_0$, (notice the minus sign), we rewrite the equations of motion as

$$\frac{dq}{d\tau} = p, \tag{11}$$

$$\frac{dq}{d\tau} = -q + I_c F(q, \tilde{\rho}(q)), \tag{12}$$

where we have introduced the current parameter

$$I_c = \frac{e^2 N}{2\pi \nu_s E_0 \sigma_{\delta 0}}, \tag{13}$$

and written the collective force contribution as

$$F(q, \tilde{\rho}(q)) = -\int_{-\infty}^{\infty} \tilde{W}(q - q') \tilde{\rho}(q') dq', \tag{14}$$

$$F(q, \tilde{\rho}(q)) = \hat{\omega}_0 \sum_{n=-\infty}^{\infty} e^{inq\sigma_z/R} \rho_n \tilde{Z}(n), \tag{15}$$

emphasizing the possible use of either an impedance or wake representation of the collective force. In the following sections we will use an impedance to model radiation effects (Section 3) and wake potential functions to represent the interaction of the bunches with the vacuum chamber (the pipe wall, beam position monitors, etc., Section 4).

In (15), $\tilde{W}(q) = W(z/\sigma_{z0})$ and $\tilde{\rho}(q) = \rho(z/\sigma_{z0})\sigma_{z0}$ are the wake function and bunch density expressed in terms of the scaled longitudinal distance q. The ρ_n quantity defined as $\rho_n = \int dq e^{-inq\sigma_{z0}/R} \tilde{\rho}(q)/2\pi = \int dz e^{-inz/R} \rho(z)/2\pi$ is the same as ρ_n in (8) since $\tilde{\rho}(q)dq = \rho(z)dz$. It is, $\tilde{\rho}(q) = (\sigma_{z0}/R) \sum_n e^{inq\sigma_{z0}/R} \tilde{\rho}_n$.

The beam distribution function $f(q,p)$ in phase space evolves according to the Vlasov-Fokker-Planck equation (16) reported below with the Vlasov part (LHS of equation) accounting for RF focusing and collective effects and the Fokker-Plank part modelling radiation damping and quantum excitations. With the continuing understanding that the scaling factors for the dynamical variables σ_{z0} and $\sigma_{\delta 0}$ represent the natural rms bunch and relative energy spread of a (gaussian) bunch in the low current limit, the VFP equation in the normalized variables q and p takes the form [8]

$$\frac{\partial f}{\partial \tau} + \frac{\partial f}{\partial q} p + \frac{\partial f}{\partial p} \left[-q + I_c F(q, f, \tau) \right] = \frac{2}{\omega_s \tau_d} \frac{\partial}{\partial p} \left(pf + \frac{\partial f}{\partial p} \right), \tag{16}$$

where τ_d is the longitudinal damping time. By definition $\tilde{\rho}(q) = \int f(q,p) dp$. Typically one is interested in determining stability of equilibria. Eq. (16) admits equilibria in the form

$f_0(q,p) = \tilde{\rho}_0(q)\exp(-p^2/2)/\sqrt{2\pi}$ (Haïssinski solutions) with $\tilde{\rho}_0(q)$ satisfying the Haïssinski equation $\tilde{\rho}_0' = (-q + I_c F)\tilde{\rho}_0$.

In the following we will investigate stability by solving numerically (16) using the methods described in [8]. We start either from a Haïssinski distribution and look at the solutions for deviation from equilibrium or we begin with a non-equilibrium distribution (say a 2D gaussian) and integrate over a few damping times looking for convergence (or lack of convergence) to equilibrium.

For some of the collective forces considered in the following, notably those deriving from radiation effects, it is possible to derive a fairly accurate estimate the current threshold by studying the linearized Vlasov equation and invoking the Boussard criterion. The Boussard criterion states that if the wavelength of the unstable modes is smaller than the bunch length and their growth time is short compared to the synchrotron period, the stability condition is the same as for that of a coasting beam provided that peak current of the bunched beam and current of the coasting beam be the same.

One is then led to linearize the Vlasov equation Eq. (16) with the RHS set to zero) around the equilibrium taken as that of a coasting beam with gaussian distribution in the energy spread. Linearization is done upon dropping in (16) the linear term in q responsible for RF focusing. Assuming that the collective force $F(q,\tilde{\rho}(q))$ be expressed in terms of an impedance the resulting linear equation yields a dispersion equation that in the normalized variables reads[‡]:

$$\frac{I_c\hat{\omega}_0}{\sqrt{2\pi}}\left(\frac{R}{\sigma_{z0}}\right)^2\frac{Z(n)}{n} = \frac{i}{W_D(\omega R/(\omega_s\sigma_{z0}n))}, \tag{17}$$

where for Im $\Omega > 0$ the function $W_D(\Omega)$ is defined as the integral

$$W_D(\Omega) = \frac{1}{\sqrt{2}\pi}\int_{-\infty}^{\infty}\frac{e^{-p^2/2}pdp}{p-\Omega} \tag{18}$$

and for Im $\Omega < 0$ by its analytical continuation.

$W_D(\Omega)$ can be expressed in terms of the so-called error function of complex argument $w(z) \equiv e^{-z^2}\mathrm{erfc}(-iz) \equiv e^{-z^2}\,[1 + 2i/\sqrt{\pi}\int_0^z \exp(\xi^2)d\xi]$. We have $W(z) = 1 + iz\sqrt{\pi/2}w(z/\sqrt{2})$ [9].

In Eq. (17) the quantity ω is the frequency of the mode with wavelength $\lambda = 2\pi R/n$. The current threshold for instability is defined as that value above which (17) admits solutions with ω having a positive imaginary part (corresponding to modes with exponentially increasing amplitude). Because $|W(\Omega)| \leq 1$ when Im $\omega = 0$, a necessary condition for the existence of unstable solutions to the linearized Vlasov equation is that $(I_c\hat{\omega}_0/\sqrt{2\pi})\,(R/\sigma_{z0})^2\,|Z(n)/n| \geq 1$. By setting the LHS of the last inequality to unity one obtains a conservative estimate of the instability threshold, which is often used for a first quick assessment (Keil-Schnell criterion). Alternate ways of writing the Keil-Schnell equation are ($\beta_0 = 1$):

[‡]From now on we drop the ˜ from the notation of Z as a function of n.

$$\frac{e\hat{I}}{2\pi|\eta|\sigma_{\delta 0}^2 E_0}\left(\frac{R}{R_{\rm av}}\right)\left|\frac{Z(n)}{n}\right|_{\rm max}=1, \tag{19}$$

$$\frac{N}{\sqrt{2\pi}|\eta|\sigma_{\delta 0}^2\gamma_0}\frac{r_e}{\sigma_{z0}}\left(\frac{R}{R_{\rm av}}\right)\frac{2}{Z_0}\left|\frac{Z(n)}{n}\right|_{\rm max}=1, \tag{20}$$

where $\hat{I}=eNc/\sqrt{2\pi}\sigma_{z0}$ is the peak current for a gaussian bunch of rms length σ_{z0}, $r_e=2.82\times10^{-15}$ m the classical electron radius, and $Z_0\simeq(\mu_0/\epsilon_0)^{1/2}=120\pi\ \Omega$ (MKS) the vacuum impedance.

Sometimes, instead of taking for $|Z(n)/n|$ its maximum value for varying n the prescription is given that $|Z(n)/n|$ should be evaluated at a mode number n corresponding to a wavelength comparable to the bunch size, *i.e.* $k\simeq 1/\sigma_{z0}$ or $n=2\pi R/\lambda\simeq R/\sigma_{z0}$. The corresponding Keil-Schnell equation then would read:

$$\frac{\sqrt{2}N}{\sqrt{\pi}|\eta|\sigma_{\delta 0}^2\gamma_0}\frac{r_e}{R_{\rm av}}\frac{|Z(n=2R/\sigma_{z0})|}{Z_0}=1 \tag{21}$$

Because the Keil-Schnell equation in the form (21) or variations thereof[§] is often applied to bunched beams well beyond the conditions of validity of the Boussard criterion, it will be interesting in the following to compare its predictions against the more accurate analysis discussed in this Report.

Outside the domain of applicability of the Boussard criterion and short of solving the VFP in time domain, evaluation of the current threshold from the linearized Vlasov equation for bunched beams requires a more sophisticated treatment involving the expansion of the bunch distribution in azimuthal and radial modes. There are codes carrying out this procedure [10] that have been used successfully. However, problems of convergence with the order of truncation of the mode expansion have occasionally been experienced [11] casting some reservations on the general reliability of the method. An improvement on the mode-expansion analysis using slightly different methods are currently underway [12, 13] and will also be applied to the MDR in the next future.

3 Radiation Impedances

Although experimental evidence is relatively new, emission of coherent synchrotron radiation by electron beams in electron storage rings has since long been predicted. More recent is the realization that CSR can cause harmful longitudinal instabilities. The physics of this instability is well understood being essentially the same mechanism behind the functioning of the free electron lasers. In a curved trajectory radiation emitted from trailing particles within a bunch can overtake particles in the front. While incoherent SR radiation has negligible effects, under the right conditions the forces exerted by the coherent part of radiation can become noticeable. Much of the low-end of the radiation spectrum is suppressed by the

[§]Sometimes it is suggested that one should take the average of $|Z/n|$ over the bunch spectrum.

metal shielding of the vacuum chamber but radiation with frequency above shielding cut-off, typically corresponding to a wavelength of the order of the bunch length or smaller, will cause a charge modulation on the bunch with the same wavelength if the beam current is sufficiently large. In turn, this charge modulation will act as source of radiation at that wavelength and initiate a feed-back process that can rapidly lead to a disruption of the initial bunch distribution.

The shielding cut-off becomes effective for wavelengths larger than

$$\lambda_0 = 2h(h/R)^{1/2} \tag{22}$$

where h as the vacuum chamber height and R the radius of curvature of the particle orbit. This is smaller than the usual waveguide cut-off by the factor $(h/R)^{1/2}$. In the model used to derive this expression - the one that will be used in this section to estimate the CSR impedance in the bending dipoles - shielding is approximated by a pair of perfectly conducting parallel plates at distance h and the particles are assumed to follow a circular path of radius R. Estimates for alternate geometries of the vacuum pipe cross-section (rectangular, circular ...) differ by a numerical factor of order unity upon a suitable interpretation of h as representing the transverse dimension [14]. The same parallel plate model yields an estimate of the maximum real part of the radiation impedance Re $Z(n)/n$ as

$$\left.\frac{\text{Re } Z(n)}{n}\right|_{\max} \simeq Z_0 \frac{h}{R} e^{-\pi/3} \simeq 132.3 \frac{h}{R} \quad (\Omega). \tag{23}$$

The maximum occurs at $n_{\max} \equiv 2\pi R/\lambda_{\max} = \pi\sqrt{2}(R/h)^{3/2}$ or $\lambda_{\max} = \lambda_0/\sqrt{2}$. By contrast, at $\lambda = \lambda_0$, with λ_0 as defined above or $n_0 = \pi(R/h)^{3/2}$, the ratio Re $Z(n)/n$ is 70% of its peak value. For $\lambda = (\pi/\sqrt{2})\lambda_0$, one finds that Re $Z(n)/n$ is less than 10^{-3} times its maximum. For all purposes this latter expression can be taken as definition a critical wavelength above which radiation is effectively zero.

A closed form expression for the complete CSR impedance can be written for the parallel plate model in terms of series of Bessel functions.

$$Z(n,\omega) = Z_0 \frac{(\pi R)^2}{\beta_0 h} \sum_{p=1}^{\infty} \Lambda_p \cdot \left[\frac{\omega\beta_0}{c} J'_{|n|} H^{(1)\prime}_{|n|} + \left(\frac{\alpha_p}{\gamma_p}\right)^2 \frac{n}{R} J_{|n|} H^{(1)}_{|n|} \right] . \tag{24}$$

Here $H^{(1)}_n = J_n + iY_n$, where J_n and Y_n are Bessel functions of the first and second kinds, $\alpha_p = \frac{\pi p}{h}$, $\gamma_p^2 = (\frac{\omega}{c})^2 - \alpha_p^2$. The argument of the Bessel functions is understood to be $\gamma_p R$. The sum on p corresponds to modes in the Fourier expansion with respect to the vertical dimension y. The factor Λ_p depends on but is not very sensitive to the detailed profile of the vertical beam distribution $H(y)$. For this study we used a square step distribution constant for $y \in [-\delta h\ ,\ \delta h]$ and zero otherwise, we have $\Lambda_p = 2(\sin(x)/x)^2,\ \ x = \alpha_p \delta h/2$ for odd p and zero for even p. As δh is very small compared to h, Λ_p depends very weekly on δh.

We termed 'complete impedance' the quantity $Z(n,\omega)$ with distinct dependance on frequency and mode number. What is usually called impedance and used in the calculation of dynamics is $Z(n,\omega)$ evaluated at $\omega = n\hat{\omega}_0$, $Z(n) = Z(n, n\hat{\omega}_0)$ where $\hat{\omega}_0 = \beta_0 c/R$. By doing

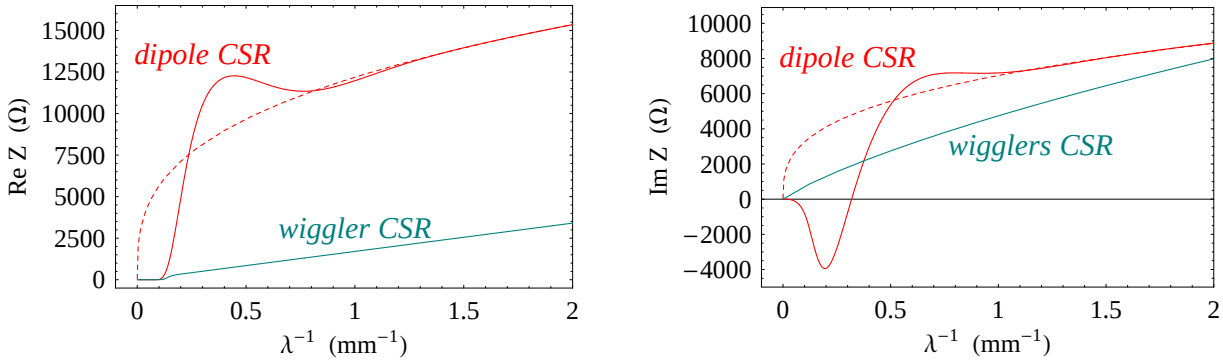

Figure 1: Real (figure to the left) and imaginary (figure to the right) part of the CSR impedances $Z(n)$ due to dipoles only with (solid red lines) and without (dashed red lines) shielding. The wiggler impedance is for free space but the real part was multiplied by an attenuation factor to model shielding effects, as explained in the text.

so one neglects some of the retardation effects associated with radiation emission. The idea behind this approximation is that only components of the electric field having phase velocity close to particle velocity will have appreciable effects on the beam.

We modelled the action of CSR in the MDR dipoles by using (24) with $R = R_d$ interpreted as the local radius of curvature of the particle orbit in the bends. In other words, the CSR induced potential is calculated as if the particles followed a circular path of radius R_d. While we expect that this approximation will give an acceptably accurate estimate of the potential difference due to CSR over one turn, transition effects as the bunches enter and exit the dipoles are obviously lost in this model.

In the MDR lattice most of the bending (323.7^0) takes place in the 2 m length dipoles in the arc cells, with 20.18 mrad bend angle and 10 m radius of curvature. Additional bending (total of 46.3^0) takes place in the dipoles providing the matching into the straight sections (1.8 m length, 10.09 mrad bending angle, 18 m radius of curvature). The bending excess $(323.7^0 + 46.3^0) - 360^0 = 10^0$ is compensated by a small offset of the quadrupoles in the arc cell. In our calculation we assumed for R_d the value of the prevalent radius of curvature *i.e.* $R_d = 10$ m without trying to account for the larger values in the matching dipoles and erring on the conservative side as a larger R_d tames CSR effects (see (23)). We accounted for shielding by the 2 cm radius pipe by setting $h = 4$ cm. With this choice of parameters we have $\lambda_0 = 5.0$ mm (wavelength where fields start to roll off due to shielding), $(\pi/\sqrt{2})\lambda_0 = 11.2$ mm (wavelength above which radiation is effectively zero), and $\lambda_{\max} = 3.5$ mm (wavelength where Re $Z(n)/n$ is maximum.

Plots of the real and imaginary part of the radiation impedance Z_d due to the dipole impedance with the parallel plate model are reported in the pictures of Fig. 1 (solid red lines). For comparison we also plotted the free-space radiation impedance [6, 15] ($\beta_0 = 1$):

$$Z_d^{\text{free}}(k) = Z_0 \frac{\Gamma(2/3)}{3^{1/3}2}(\sqrt{3} + i)(kR_d)^{1/3} \tag{25}$$

with $k = n/R_d$. This expression is related to the expression $\hat{Z}_d^{\text{free}}(k)$ reported in [6] by

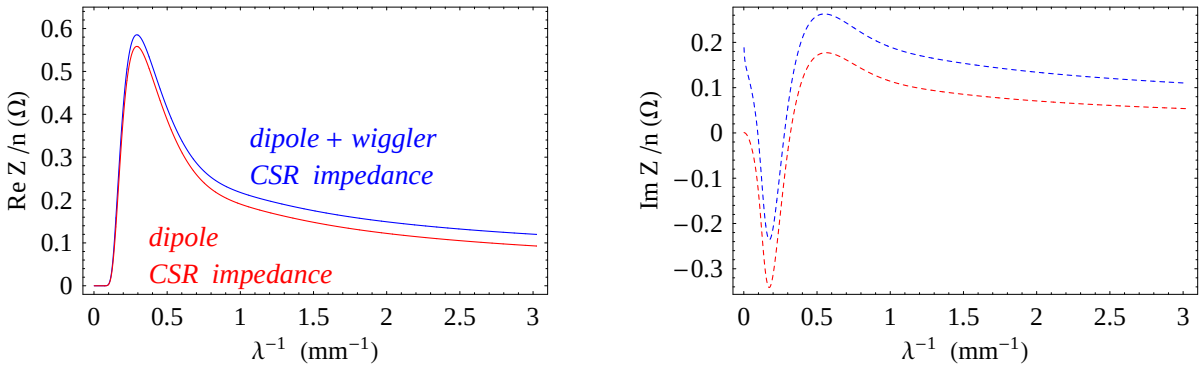

Figure 2: Real (figure to the left) and imaginary (figure to the right) part of the CSR impedance $Z(n)/n$ due to dipoles only (red lines) and dipole + wigglers (blue lines).

$Z_d^{\rm free}(k) = (Z_0 c/4\pi)(2\pi R_d/c)\hat{Z}_d^{\rm free}(k)$. One can observe that the shielded approaches the unshielded impedance for high frequencies as the vacuum cross section becomes large compared to the radiation wavelength and the two are essentially the same for wavelengths smaller than 1 mm.

In the MDR wiggler insertions are responsible for most of the radiation loss and one would expect a significant contribution to the overall CSR effects. While CSR effects due to wigglers are indeed noticeable the corresponding impedance at low frequency – relevant for stability analysis, turns out to be a relatively small fraction of that associated with radiation emission in the dipoles.

In estimating the effect of wigglers we make use of the low-frequency limit for the radiation impedance per unit length in an infinitely long insertion reported in [7], Eq. (26)

$$\hat{Z}_w = \pi k_w \frac{k}{k_0}\left[1 - \frac{2i}{\pi}\log\left(\frac{k}{k_0}\right)\right] \qquad \text{(cgs units)}, \tag{26}$$

where $k_w = 2\pi/\lambda_w$, is the wiggler wavenumber, λ_w is the period, k_0 the fundamental wave number, $k_0 = 2\gamma_0^2 k_w/(1 + K^2/2)$, with γ_0 being the relativistic factor and $K \simeq 93.4 B_{w0}\lambda_w$ the wiggler parameter; B_{w0} is the wiggler peak field.

We should recall that the quantity (26) as given by J. Wu *et al.* is not an impedance in the sense of Eq. (5), having been defined as the Fourier transform of the longitudinal electric field per unit charge (not of the wake potential). The conversion from $\hat{Z}_w$ to the conventional expression is

$$Z_w(n) = L_w \frac{Z_0 c}{4\pi}\frac{1}{\beta_0 c}\hat{Z}_w(k)\Big|_{k=n/R_d} \qquad \text{(MKS units)}, \tag{27}$$

where L_w is total length of the wiggler insertions. For comparison with the CSR dipole impedance, we chose to express the wave number $k = 2\pi/\lambda = n/R$ with respect to the radius $R = R_d$. Recall that any choice for R is legitimate: a different value for R would merely redefine the meaning of the mode number n.

For the purpose of stability analysis use of the limiting low-frequency expression (26) is adequate. Comparison against a numerical calculation [7] shows that (26) is accurate for

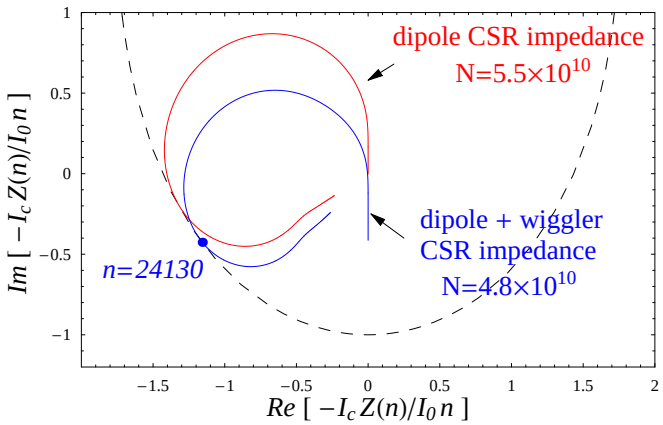

Figure 3: Keil-Schnell beam stability diagram in the presence of CSR impedance alone. The dashed curve delimits the stability region (the area including the origin). The solid curves represent $I_c Z(n)/nI_0$ for varying mode number n at threshold, where $I_0 = \sqrt{2\pi}(\sigma_{z0}/R)^2/\omega_0$. The blue (red) line includes the contribution from both dipoles and wigglers (dipoles only). The critical number of particles/bunch for stability is also reported for the two cases. The mode number $n = 24130$ (corresponding to a wavelength $\lambda = 2$ mm) is in the vicinity of the modes that go unstable at the crossing of current threshold.

$k \leq 0.1k_0$. As $k_0 \simeq 5 \times 10^5$ the above expression is expected to be accurate for wavelength λ larger than 0.1 mm. This is much smaller than $\lambda \simeq 2$ mm of the unstable modes that we found at the crossing of threshold, suggesting that use of (26) is appropriate when doing the linear analysis and is comparable to (although still smaller than) the resolution (about 0.16 mm) of a typical 400×400 phase-space grid we used in the VFP solver.

A limitation of (26) is that it does not account for shielding effects. One would expect that an attenuation of radiation exponential with the wavelength around a cut-off comparable to (22) would apply to SR emission from a wiggler as well. For the analysis presented in this Report we multiplied the real part of $Z_w(n)$ by an attenuation factor of the form $[\tanh(6.8(n - n_{w0})/n_{w0}) + 1]/2$ where the numerical value 6.8 was chosen to give a slope comparable to that of Re Z_d and $n_{w0} = \pi(R_w/h_w)^{3/2}$ is a mode-number cut-off written in analogy with the dipole mode-number cut-off n_0, with $h = 1.6$ cm and $R_w = 3.3$ m being the radius of curvature of the orbit in the wiggler in correspondence to the wiggler magnetic field peak value B_{w0}. The corresponding wavelength $\lambda_{w0} = 2\pi R_w/n_{w0} = 5.6$ mm.

In analogy with the dipole CSR impedance one would expect that the effect of shielding on the imaginary part of the wiggler impedance be somewhat more complicated than the exponential attenuation experienced by the real part. In our calculations we will make no attempt to account for shielding on Im $Z_w(n)$ and content ourselves with the expression (27) in free space. In doing so we will likely overestimate Im $Z_w(n)$ for small n. While this should have no direct impact over the linear stability analysis (the unstable modes are shown to have wavelength of about 2 mm where the free space approximation for the impedance is more accurate as it is well below the shielding cut-off wavelength $\lambda_{w0} = 5.6$ mm,), there is an indirect but small effect through potential well distortion. Indeed, we find that the

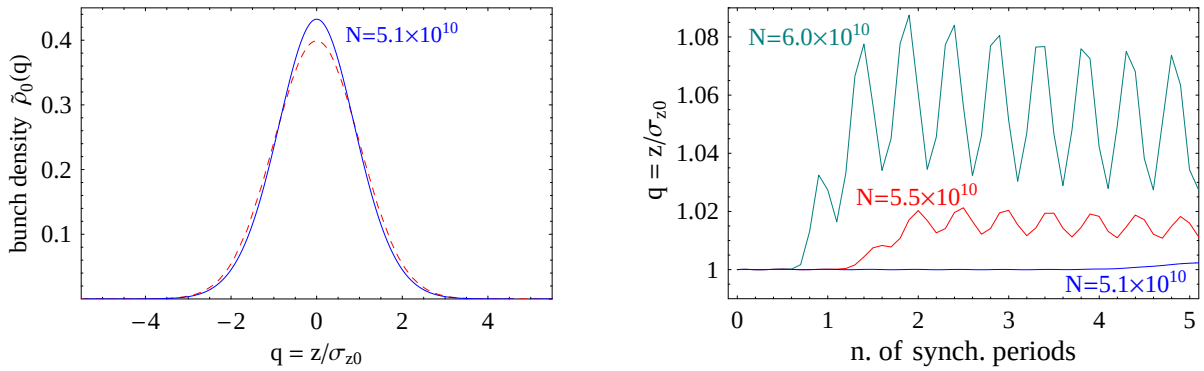

Figure 4: Figure on the left: bunch equilibrium in the presence of the sole CRS impedance for $N = 5.1 \times 10^{10}$ (slightly above threshold) The dashed line represents the gaussian equilibrium in the zero-current limit. Figure on the right: evolution of the relative energy spread in units of natural relative energy spread, $\sigma_p = \sigma_\delta/\sigma_{\delta 0}$, for varying bunch population N in the presence of CSR (from both dipoles and wigglers) and starting from a Haïssinski equilibrium. The critical N for instability is in the range $N = 5.02 - 5.05 \times 10^{10}$.

reactive part of the free-space wiggler CSR impedance causes a few percent decrease in the rms length of the bunch equilibrium or correspondingly a few percent increase in the peak current value. This distortion, if not physical, would lead to a more pessimistic estimate of the threshold for instability by the same relative amount of few percent.

A Haïssinski equilibrium in the presence of CSR effects alone is shown in the left picture of Fig. 4 for a current just above instability threshold. The profile is symmetric – a reflection of the fact that only the imaginary part of the impedance is contributing to the distortion as the low frequency part of ReZ is cut off by shielding.

We determined the current threshold for instability from the linear Vlasov equation by constructing a Keil-Shnell diagram as shown in Fig. 3. The stability boundary (dashed line in the picture) corresponds to the parametric plot of the RHS of Eq. (17) obtained by setting Im $\omega = 0$ and letting Re ω vary from $-\infty$ to $+\infty$. In the same picture we also report the curves corresponding to the LHS of (17) for varying mode number n for the case in which only CSR from the dipoles is included $Z = Z_d$ (red line) and the case with both dipoles and wigglers contributing $Z = Z_d + Z_w$ (blue line). The fact that the two curves are tangent to the stability boundary qualifies the corresponding values for I_c as the critical current parameter for instability. In terms of number of particles per bunch we found $N = 4.8 \times 10^{10}$ to be the critical value for the case $Z = Z_d + Z_w$. This estimate is for the peak current of a $\sigma_{z0} = 5.5$ mm gaussian bunch. Accounting for the increase in the peak current due to potential well distortion would lower the estimate to about $N = 4.5 \times 10^{10}$. The same linear analysis also predicts that the wavelength of the modes that first go unstable at the crossing of threshold is $\lambda \simeq 2$ mm, about a factor 2 smaller than the cut-off wavelength λ_0.

Numerical solutions of the VFP equation starting from a Haissinki equilibrium place the estimate of the instability threshold in the range $N = 5.02 - 5.05 \times 10^{10}$, a value about 10% larger than the one resulting from the linear analysis (after accounting for the bunch

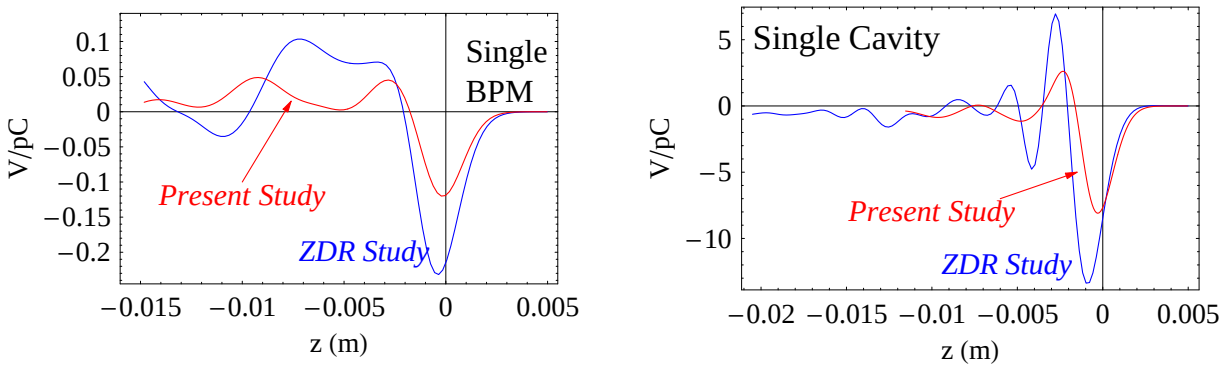

Figure 5: Comparison between the models of wake functions for a single RF cavity and BPM used in the present study (red lines) and those used for the study reported in the ZDR for NLC [3].

distortions). We attribute the difference to the effect of finite bunch-size (recall that Eq. (17) was derived under the costing-beam approximation). Previous numerical work showed that the VFP solver used in the calculation very accurately reproduces the value predicted by the linear theory when applied to coasting beams [8]. The presence of instability is detected by looking at variation over time in the rms energy spread starting from an equilibrium distribution. The growth rate for a CSR driven instability is relatively fast and develops very quickly (within a couple of synchrotron periods) for currents just above threshold (see Fig. 4).

A cruder but still not too far-off estimate can be obtained from the Keil-Schnell equation (20). On the assumption that we can neglect the contribution from the wigglers and $|Z(n)/n| \simeq |\mathrm{Re}\ Z(n)/n|_{\max} \simeq Z_0 e^{-\pi/3} h/R$, (see Eq. (23))

$$N_{\mathrm{thr}} \simeq 3.6 \left(\frac{R_{\mathrm{av}} \sigma_{z0}}{r_e h} \right) |\eta| \sigma_{\delta 0}^2 \gamma_0 = 4.2 \times 10^{10}, \tag{28}$$

where the numerical factor is $e^{\pi/3}\sqrt{\pi/2} \simeq 3.6$. This threshold value is about 25% smaller than $N = 5.5 \times 10^{10}$, the value derived by accurate solution of (17) when the wiggler CSR is neglected (Fig. 3, red line). Note that, interestingly, the above simplified criterion of instability does not depend on the radius of curvature - only the average machine radius.

A comparison with [4] shows that the estimate presented there is somewhat more pessimistic. Because in [4] the impedance is unshielded there is no clear identification of the wavelength of the unstable modes. A conservative choice as made in [4] is to suggest for the critical wavelength the shielding cut-off λ_0, for which the reported estimate of the threshold is $N = 3.3 \times 10^{10}$¶. However at $\lambda = \lambda_0$ the unshielded $|Z/n|$ is noticeable larger than the shielded $|Z/n|$ at $\lambda = 2$ mm where our analysis places the critical wavelength - hence explaining our more optimistic estimate of the threshold. There is, of course, a certain degree of uncertainty about the accuracy of the parallel-plate model used in our calculation, which

¶This is in the presence of dipole CSR only. Our estimate for this case is $N = 5.5 \times 10^{10}$.

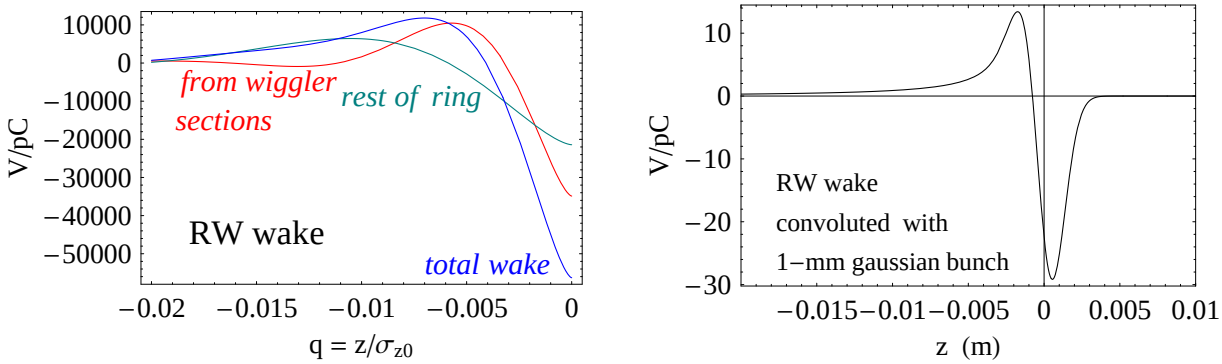

Figure 6: Resistive-wall (RW) wake function broken down to the components coming from the wiggler sections and from the rest of the ring (figure on the left). The figure on the right reports the total RW wake function convoluted with a 1-mm gaussian bunch profile; this is the model of RW wake function used in the present calculations. Notice the different scales in the horizontal axis.

possibly is only a rough approximation of the actual shielding effect provided by the vacuum chamber. It is conceivable that the value provided here and that reported in [4] may represent the high and low end of a likely range for the instability threshold.

4 RF Cavities, BPM's, and Resistive wall

In evaluating the collective effects by the vacuum chamber for the present study we included the RF cavities, BPM's, and resistive wall.

The wake functions for the cavities and BPM were calculated by Cho Ng using MAFIA [16]. The design of these components was based on the design reported in [3], to which we refer for a description, except for the a larger value of the pipe radius (from $b = 1.25$ cm to $b = 1.6$). The wake functions were computed by evaluating the longitudinal electric field driven by a finite size (1-mm rms gaussian) rigid charge source. As a result causality is violated and the wake functions are non-zero for $z > 0$. We did not attempt in our study to restore causality by artificially removing (or moving) the $z > 0$ part of the wake as there is no clear prescription for doing so.[‖] A sensible thing to do in future studies would be to produce wakes generated by shorter bunches and look for convergence of results when looking at the dynamical effects on beams. A sensitivity study where artificial perturbations are added to the computed wakes could also be useful. However, there exist already calculations [11] for earlier design of the MDR vacuum chamber components showing that wakes computed from a 0.5 mm driving bunch do not yield significantly different assessment of beam dynamics. The plots for individual RF cavity and BPM are reported in Fig. 5. Unfortunately, the wake data currently available are truncated beyond about 15 cm behind the bunch center.

[‖]We did, however, tried a wake function modified to restore causality in a study of the old MDR 1996 lattice, which was carried out for comparison with previous investigations – see the Appendix.

To avoid possible high frequency effects due to the truncation and preserve smoothness we artificially added a fast decreasing exponential tail (not shown in Fig. 5, but included in the left picture of Fig. 7 where the overall contribution of the 146 BPM's and 4 RF cavities is reported).

As for resistive effects, we made use of the existing analytical formula [5] for an infinitely long, straight vacuum chamber with circular cross section of radius b. The longitudinal electric field caused by the finite conductivity of the pipe wall at $z < 0$ due to a charge e at $z = 0$ is given by

$$E_z^{rw}(z,b) = -\frac{4Z_0 ce}{\pi b^2}\left(\frac{1}{3}e^u\cos(\sqrt{3}u) - \frac{\sqrt{2}}{\pi}\int_0^\infty \frac{x^2 e^{ux^2}}{x^6+8}dx\right) \quad \text{for } z \le 0, \tag{29}$$

with $u = z/(2\chi)^{1/3}b$ and $\chi = 1/Z_0\sigma b$ where σ is the conductivity of the vacuum chamber. For Aluminum at room temperature $\sigma = 3.5 \times 10^7\ \Omega^{-1}\mathrm{m}^{-1}$.

As it is expected that the vacuum chamber in the straight $L_w = 62$ m sections accommodating the wiggler insertions will be significantly narrower than in the rest of the machine ($b = b_w = 0.8$ cm *vs.* $b = b_a = 2$ cm) we wrote the resulting wake function for the resistive wall as the sum of the two contributions

$$W^{rw}(z) = L_w E_z^{rw}(z, b_w)/e + (C - L_w)E_z^{rw}(z, b_a)/e, \tag{30}$$

(obviously $W(z) = 0$ for $z > 0$). The plot of (30) together with that of the two components indicated in the RHS is reported in the left picture of Fig. 6.

We did not, however, use directly (30) in our calculation but we first convoluted it with a 1-mm rms gaussian source in analogy with the way the wake functions for the other components of the vacuum chamber were determined. We thought this to be justified after a comparison between a calculation of beam dynamics done with the wake as in (29) and a calculation done with the above-mentioned convolution. No other sources of collective effects were included. The only noticeable dynamical effect found was potential well distortion while no instability was detected up to the largest bunch population considered ($N = 150 \times 10^{10}$). At the largest N the two resulting bunch profiles while looking very non-gaussian were nonetheless very similar to each other.

For fast evaluation in the VFP solver we tabulated the integral on the RHS of (29) for $|u| \le 6$ and used a 3rd order interpolation, while for $|u| > 6$ we used an approximation retaining the first two terms of its asymptotic expansion (keeping more terms in this expansion turns out to make the approximation worse for moderate $|u|$):

$$\int_0^\infty \frac{x^2 e^{-|u|x^2}}{x^6+8}dx \;\simeq\; \frac{\sqrt{\pi}}{32}|u|^{-3/2} + \frac{105\sqrt{\pi}}{2048}|u|^{-9/2}. \tag{31}$$

The resulting approximation was found to yield a relative error of 10^{-3} or smaller.

The profile of the total wake function summing up the contribution from 4 RF cavities, 146 BPM's, and the resistive wall contribution (convoluted wake) is shown in Fig. 7. For sake of completeness we also report the corresponding impedance obtained by taking the

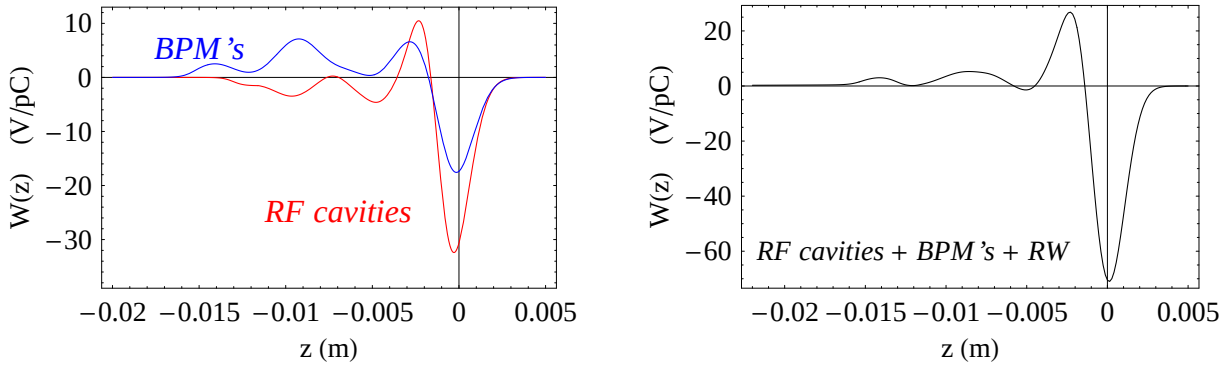

Figure 7: Wake functions for the BPM's and RF cavities (figure on the left) and total wake function including contributions from BPM's, cavities, and resistive wall.

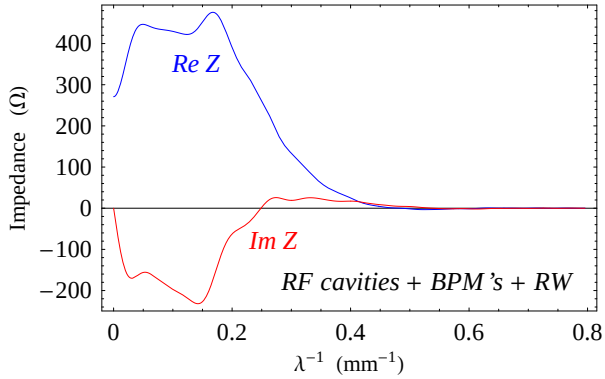

Figure 8: Impedance corresponding to the wake function of Fig. 7 (right picture) including contributions from BPM's, cavities, and resistive wall.

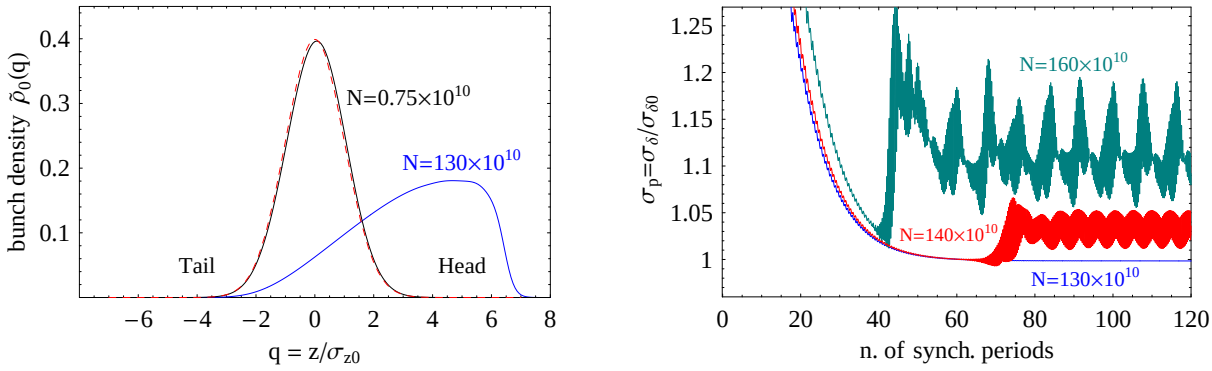

Figure 9: Figure on the left: Haïssinski equilibrium distribution at nominal bunch population $N = 0.75 \times 10^{10}$ and right below instability threshold $N = 130 \times 10^{10}$. The dashed (gaussian) curve represents the bunch distribution in the limit of vanishing current. Figure on the right: evolution of the (normalized) relative energy $\sigma_p = \sigma_\delta/\sigma_{\delta 0}$ starting from a gaussian distribution far from equilibrium. Threshold for instability is in the range $N = 133 - 136 \times 10^{10}$.

Fourier transform of the wake in Fig. 7 although no use of such an impedance was made to calculate the beam dynamics.

In studying stability with the VFP solver we started with initial gauss distributions far from equilibrium (with rms length and relative energy spread two time larger than the natural values in the zero current limit) and we let them evolve over several damping times. This is more time consuming than starting from a Haïssinski equilibrium but was necessary because the algorithm used to solve the Haissinki equation failed to converge for currents at which instability takes place.

As in the previous section we detected instability by inspecting the evolution of the rms energy spread over time. In a situation of equilibrium σ_δ converges to the natural value $\sigma_{\delta 0}$ as a result of radiation damping. Above threshold damping is interrupted by sudden jumps (see right picture in Fig. 9). The thick bands visible in the picture are the envelope of rapid quadrupole-like oscillations that are triggered by the instability. Our numerical estimate for the threshold is a fairly large $N = 133 - 136 \times 10^{10}$, more than two orders of magnitude above the design value.

Variations in the numerics of the VFP solver (mesh size, time step) were not found to cause significant deviations in the solutions.

Before ending this section we examine the threshold as predicted by the simplified equation (21). One finds that the vacuum chamber impedance evaluated at $k = 1/\sigma_{z0}$ or $\lambda^{-1} = 1/2\pi\sigma_{z0} = 0.029$ mm^{-1} is about $|Z| \simeq 420\ \Omega$ with relatively little variation ($270 - 500\ \Omega$) over the range of the bunch spectrum. With this value for the impedance in (21) we find an estimate for the threshold $N = 9.7 \times 10^{10}$ about 15 times smaller than the value obtained from numerical solution of the VFP equations. Needless to say such a large discrepancy makes use of (21) dubious at the very least.

To make contact with conventional notation we report the value $|Z/n^*|$ at $k = 1/\sigma_{z0}$ where $n^* = R_{\rm av}/\sigma_{z0} \simeq 8700$ is the usual mode number expressed in terms of the *average* ring radius. We have $|Z/n^*| \simeq 0.05\ \Omega$.

5 Conclusions

The main result of our study is a confirmation that instability thresholds for the new MDR Feb. 03 lattice should be safely above the nominal current of 0.75×10^{10} particle/bunch.

As a result of the increased momentum compaction and bunch length the instability driven by the main components of the vacuum chamber (RF cavities, BPM's, and resistive wall) is expected to appear only at exceedingly large current (more than two order of magnitude larger than nominal value). No detectable potential well distortion is expected at nominal current either.

More severe but still acceptable limitations are set by coherent radiation effects, mostly from emission occurring in the bending magnets, as wigglers contribute much of incoherent but only a small portion of coherent radiation. We find an instability threshold about 6 times the design beam current – marginally larger than the estimate reported in [4]. We believe this value to provide a safety cushion sufficient to counter the uncertainties carried by the model used to calculate the CSR effects.

Table 2: Relevant Parameters for the MDR 1996 Design.

Description	Notation	Value
Energy	E_0	1.98 GeV
Rigidity	$Brho$	6.604 Tm
Ring circumference	C	223 m
Average ring radius	$R_{\rm av}$	35.49 m
Revolution frequency	$\omega_0/2\pi$	1.345 MHz
Pipe radius (except wiggler sections)	b	1.25 cm
Momentum compaction	α	4.65×10^{-4}
Synchrotron frequency	$\omega_s/2\pi$	5.147 KHz
Synchrotron tune	ν_s	0.00382
Natural bunch length	σ_{z0}	3.9 mm
Natural rms relative energy spread	$\sigma_{\delta 0}$	0.9×10^{-3}
Longitudinal damping time	τ_d	2.5 ms
Harmonic number	h_n	532
RF voltage	$\hat{V}_{rf}$	MV
RF frequency	$\omega_{\rm rf}/2\pi$	714 MHz
Number of cavities		2

6 Appendix: Stability Study for the 1996 Lattice Design

Stability analysis in the study reported in [3] was carried out by analyzing the linearized Vlasov equation for bunched beams using the mode decomposition method as implemented in Oide's code [10]. We thought it would be interesting to carry out a cross validation against the methods used in our investigation by applying our VFP solver to the old MDR design.

Only the vacuum chamber wakes were considered.

From the perspective of this study the main differences between the 1996 and current MDR lattice are in the momentum compaction (now larger by about factor 4) and ring circumference (now 300 m *vs.* 220 m). For a list of other relevant parameters see Table 2. The new lattice is expected to have a larger number of BPM's and RF cavities; a longer circumference would also enhance resistive wall effects. However, the contribution of the individual components is smaller in the new ring because of the larger pipe radius. As a result, the total wake functions in the two cases look similar (compare Figs. 7 and 10).

When applied to the wake function shown in Fig. 10 our VFP solver shows a threshold located just below $N = 10 \times 10^{10}$ (see Fig.11).

The study reported in [3] mentions a range of values for instability threshold as the total wake was modified in different ways in an attempt to restore causality. A strong instability is reported in the range $N = 7 - 8 \times 10^{10}$ and the presence of "slow" instabilities is also detected for a number of particles as low as $N = 1.65 \times 10^{10}$ for the " capacitive" model of wake function. By "capacitive" model the authors of [3] mean a modification of the original

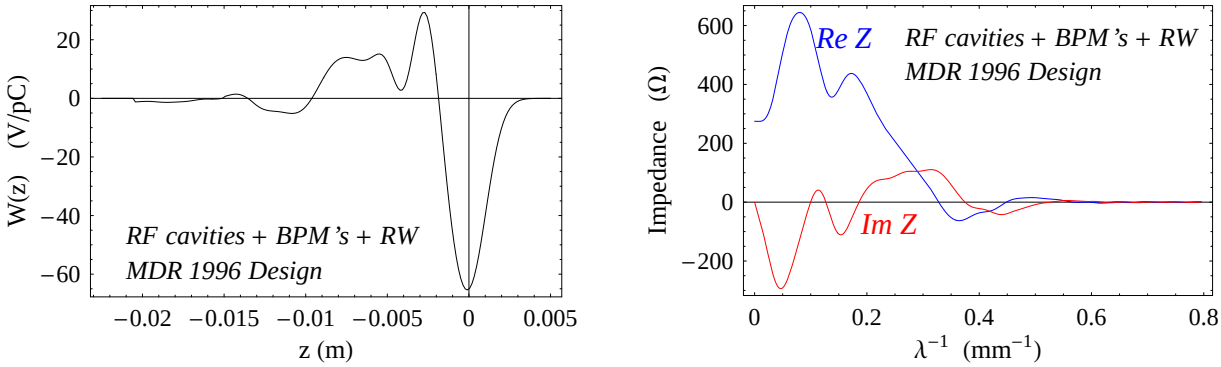

Figure 10: NLC 1996 main damping ring design. Wake function (figure on the left) comprises RW, cavities, and BPMS. The corresponding impedance as a function of the inverse of wavelength is reported in the figure on the right.

wake function as shown in the left picture of Fig. 10, that removes the $z > 0$ part by folding it symmetrically behind the ordinate axis [11]. In Oide's code [10] the calculation does not include the taming effect of radiation damping, which is accounted for "by hand". The current threshold is defined as that value at which the growth rate of the most unstable collective mode equals the inverse of the radiation damping time. As a result the values quoted in [3] should be directly comparable to the estimates reported in the present report. However, we also did some runs excluding the Fokker-Planck part of Eq. (16). For the old 1996 Lattice design, these runs place the threshold for instability in the range $8.25-8.5\times10^{10}$ particles/bunch (*vs.* $N = 10 \times 10^{10}$ when radiation damping is included).

We also repeated our calculation using the same "capacitive" approximation of the wake function as explained above. We found that the modified wake gives a noticeable more pessimistic estimate of the instability threshold which appears to be located close to $N = 5 \times 10^{10}$ when radiation damping is excluded and close to $N = 6.5 \times 10^{10}$ when radiation damping is included. In [3] the threshold for the strong instability in this case was $N = 7 \times 10^{10}$.

For the study discussed in this section we adopted the operational definition of instability as causing an increase of at least about 0.5% in relative energy spread (starting from equilibrium) in about two damping times (one damping time corresponds to about 12 synchrotron periods). At present in our study we did not make an attempt to investigate the nature ("weak" *vs.* "strong") of the instability by looking at the dependence of growth rate as a function of current. A closer comparison between the outcome from the VFP solver and analysis of the linearized Vlasov equation is in our plans for future work. At this point we content ourselves with the observation that the disagreement we find is within an acceptable range - considering the relatively large gap that the new lattice design places between operational current and estimated instability threshold.

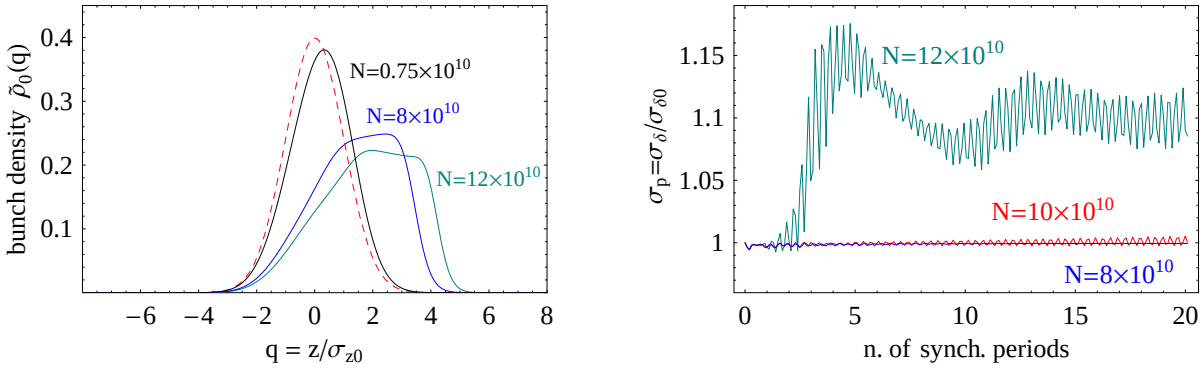

Figure 11: NLC 1996 main damping ring design. Figure on the left: Haïssinski equilibrium distributions for varying bunch population N. The dashed curve is the gaussian distribution representing the equilibrium in the limit of vanishing current. Figure on the right: evolution of the (normalized) relative energy $\sigma_p = \sigma_\delta/\sigma_{\delta 0}$ starting from Haïssinski equilibrium. Threshold for instability is just below $N = 10 \times 10^{10}$.

7 Acknowledgments

Thanks to Karl Bane and Cho Ng for providing the vacuum chamber wake functions, Andy Wolski and Bob Warnock for useful discussions.

References

[1] M. Woodley and A. Wolski, "The NLC Main Damping Ring Lattice February 2003" NLC Tech Note LCC-0113 (2003).

[2] M. Woodley, *et al.*, A Lattice with Larger Momentum Compaction for the NLC Main Damping Rings PAC01, Proceedings, PAC03 Proceedings (2003).

[3] The NLC Design Group, "Zeroth-Order Design Report for the Next Linear Collider", SLAC Report SLAC-474, Stanford, (1996).

[4] J. Wu, G. Stupakov, T. Raubenheimer, and Z. Huang, Phys. Rev. ST Accel. Beams 6, 104404 (2003)

[5] A. Chao, Physics of Collective Beam Instabilities in High Energy Accelerators, John Wiley & Sons, Inc., New York (1993).

[6] G. Stupakov and S Heifets, Phys. Rev. ST Accel. Beams **5**, 0544402 (2002).

[7] J. Wu, T. O. Raubenheimer, and G. V. Stupakov Phys. Rev. ST Accel. Beams 6, 040701 (2003).

[8] M. Venturini, R. Warnock, R. Ruth, and J. Ellison, "Coherent Synhrotron Radiation and Bunch Stability in a Compact Storage Ring", submitted for publication (2004).

[9] S. Y. Lee, *Accelerator Physics*, Chap. 3, (World Scientific, Singapore, 2000).

[10] K. Oide, Part. Accel. **51**, 42 (1995).

[11] K. Bane, private communication.

[12] R. Warnock, M. Venturini, and J. Ellison, EPAC02, Proceedings, p. 1590 (2002).

[13] R. Warnock, G. Stupakov, J. Ellison, and M. Venturini, EPAC04

[14] G. V. Stupakov and I. A. Kotelnikov Phys. Rev. ST Accel. Beams 6, 034401 (2003).

[15] J. Murphy, S. Krinsky, and R. Gluckstern, Part. Accel. **57**, p. 9-64 (1997).

[16] Cho Ng, private communication.